

11. The main sequence

11.1 Introduction

Apart from very late stages of evolution stars spend most of their life burning hydrogen on the main sequence^(11.1). Hence it is of considerable interest to understand the properties of main-sequence stars, and to describe the changes that occur as a result of hydrogen burning. A main-sequence star of somewhat special interest is the Sun: this is partly motivated by our desire to understand an object of such importance to our daily life; a more interesting consideration is that changes in the properties of the Sun over its life may have had an effect on conditions on Earth (changes in the Sun as it evolves towards the red giant stage, in approximately 7×10^9 years, will certainly have dramatic effects). From the point of view of astrophysics, the proximity of the Sun, and hence our ability to observe it in very great detail, makes it extremely important as a test of stellar evolution theory. For these reasons we return to the Sun towards the end of this chapter, after considering more general properties of main-sequence stars.

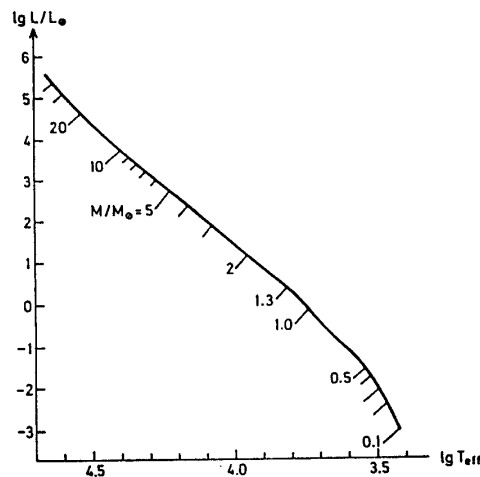


Figure 11.1. Hertzsprung-Russell diagram of the zero-age main sequence computed for the composition $X = 0.685$, $Y = 0.294$. The location of several models with masses between 0.1 and $22M_{\odot}$ are indicated below the sequence (From Kippenhahn & Weigert 1990.)

11.2 The zero-age main sequence

The zero-age main sequence (or *ZAMS*) may be defined, somewhat loosely, as the location of stars that have just settled down to hydrogen burning^(11.2). Figures 11.1 – 11.3 illustrate

^(11.1) Properly speaking *the hydrogen main sequence*. One sometimes talks about other “main sequences”, particularly for helium burning; *cf.* Chapter 12.

^(11.2) Computationally, such models may approximately be obtained by solving numerically the equations of stellar structure (9.2a) – (9.2e), without the time-derivative terms in equation (9.2c), for a homogeneous composition.

the relation between mass, luminosity, radius and effective temperature for such stars, comparing the numerical results with observed properties of binary stars (*cf.* section 2.7). The most striking feature is the rapid increase in luminosity with stellar mass, as was also predicted by the mass-luminosity relations in section 7.1. Indeed, as indicated in the figure, these relations show some similarity with the computed behaviour; in particular there is a tendency towards a steepening of the slope for masses below solar^(11.3). In contrast, the radius increases only roughly proportionally with M . Hence the effective temperature also increases substantially with increasing mass, as shown in Figure 11.1.

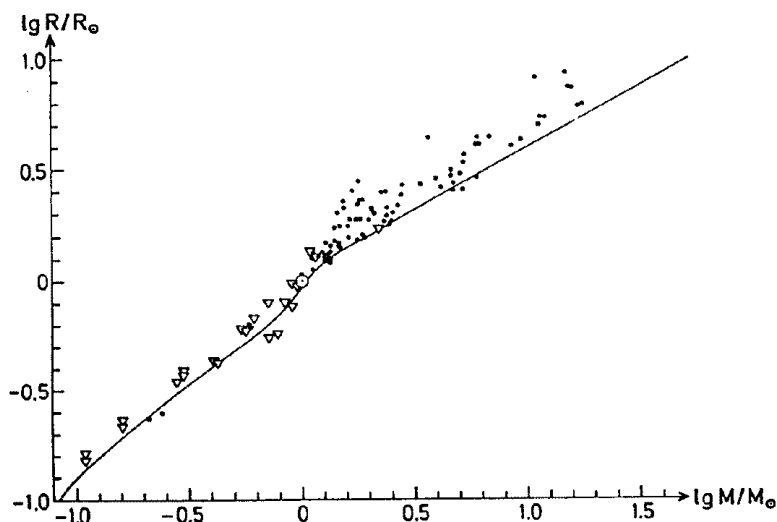


Figure 11.2. The line shows the mass-radius relation for the zero-age main sequence plotted in Figure 11.1. For comparison measured properties of binary stars are indicated by the symbols (From Kippenhahn & Weigert 1990.)

Figure 11.4 gives an indication of the interior structure of main-sequence stars. Each value of the abscissa corresponds to a given total mass of the star; a vertical slice through the diagram at that point describes the interior structure for that star. The “cloudy” areas show the location of convection zones in the models; in addition, the masses corresponding to $0.25R$ and $0.5R$, and to $0.5L_s$ and $0.9L_s$, are shown by means of continuous and dashed curves, respectively. (For example, in the star with $\log M/M_\odot = -0.4$, there is a convective envelope extending over approximately the outer 30 per cent of the mass; half of the total luminosity is generated within the inner 10 per cent of the mass, corresponding to a quarter of the radius). As discussed in Chapter 6, in low-mass stars there are extensive outer convective envelopes, which in this calculation grow to encompass the entire star at a mass of about $0.25M_\odot$. Stars of masses larger than the solar mass have convective cores, the extent of which grow rapidly with increasing mass. The reason is the increasing importance of the CNO cycle in the energy generation: because of the resulting high temperature sensitivity of the energy generation rate the energy production gets highly concentrated

^(11.3) At even lower masses, this trend is reversed; here, however, the stars have very extensive outer convection zones, and the applicability of the radiative mass-luminosity relation is certainly questionable.

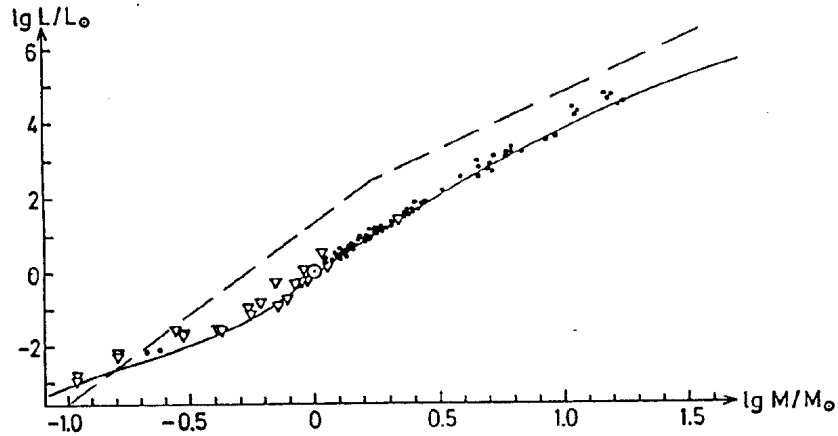


Figure 11.3. The continuous line gives the mass-luminosity relation for the zero-age main-sequence models shown in Figure 11.1. The symbols show measured properties of binary stars. For comparison, the dashed lines indicate the simple mass-luminosity relations (7.7) (assuming that $R \propto M$) and (7.8) derived in Chapter 7. (Adapted from Kippenhahn & Weigert 1990.)

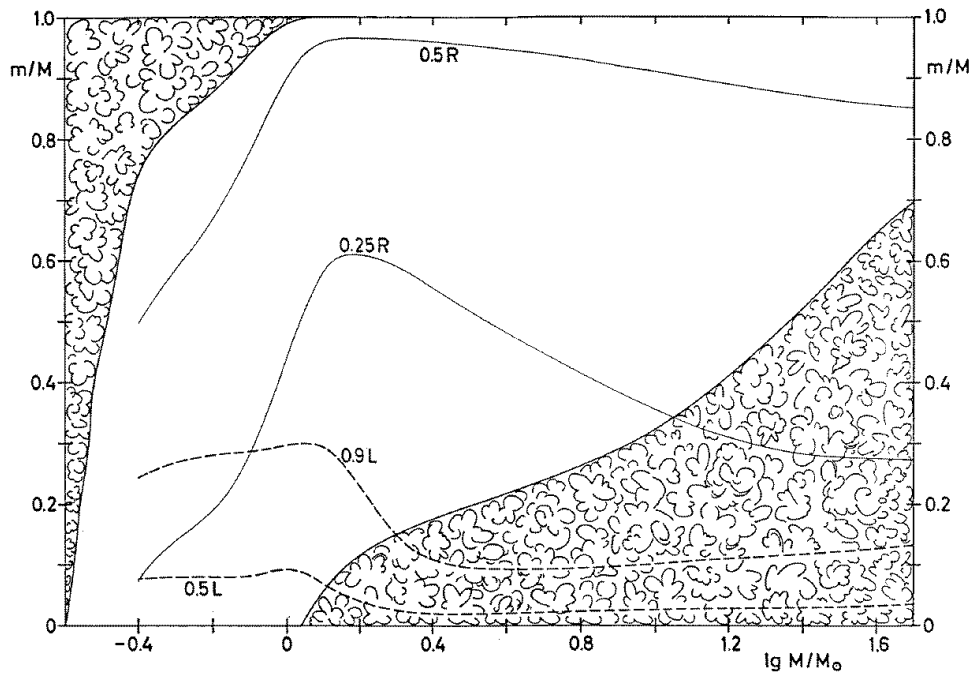


Figure 11.4. The mass values m from centre to surface are plotted against the stellar mass M for the zero-age main-sequence models which were shown in Figures 11.1 – 11.3. “Cloudy” areas indicate the extent of the convection zones inside the models. Two solid lines give the mass values at which r is $1/4$ and $1/2$ of the total radius R . The dashed lines show the mass values inside which 50 per cent and 90 per cent of the total luminosity L_s are produced. (From Kippenhahn & Weigert 1990.)

towards the centre (as is also evident from the $0.5L_s$ and $0.9L_s$ curves), and this leads to convective instability [*cf.* equation (6.19)].

11.3 Evolution during core hydrogen burning

11.3.1 The evolution in the HR diagram

Evolution tracks, from Iben's calculations, for the evolution after the ZAMS are shown in Figure 11.5. The duration of the different phases of evolution, as indicated by the numbered points on the tracks, is given in Table 11.1. Here we concentrate on the initial parts of the tracks, roughly between points 1 and 2, which correspond to the phase of hydrogen burning in the core.

Table 11.1

Interval ($i-j$)	Interval ($i-j$)				
	(1-2)	(2-3)	(3-4)	(4-5)	(5-6)
Mass (M_\odot)					
15	1.010 (7)	2.270 (5)		7.55 (4)	
9	2.144 (7)	6.053 (5)	9.113 (4)	1.477 (5)	6.552 (4)
5	6.547 (7)	2.173 (6)	1.372 (6)	7.532 (5)	4.857 (5)
3	2.212 (8)	1.042 (7)	1.033 (7)	4.505 (6)	4.238 (6)
2.25	4.802 (8)	1.647 (7)	3.696 (7)	1.310 (7)	3.829 (7)
1.5	1.553 (9)	8.10 (7)	3.490 (8)	1.049 (8)	≥ 2 (8)
1.25	2.803 (9)	1.824 (8)	1.045 (9)	1.463 (8)	≥ 4 (8)
1.0	7 (9)	2 (9)	1.20 (9)	1.57 (8)	≥ 1 (9)

Interval ($i-j$)	Interval ($i-j$)			
	(6-7)	(7-8)	(8-9)	(9-10)
Mass (M_\odot)				
15	7.17 (5)	6.20 (5)	1.9 (5)	3.5 (4)
9	4.90 (5)	9.50 (4)	3.28 (6)	1.55 (5)
5	6.05 (6)	1.02 (6)	9.00 (6)	9.30 (5)
3	2.51 (7)		4.08 (7)	6.00 (6)

The duration (in years) of different phases in the evolutionary tracks illustrated in Figure 11.5. The numbers refer to the points indicated in that figure, and the entries give the duration of the corresponding interval. Numbers in parenthesis beside each entry give the power of ten with which that entry is to be multiplied. For example, the duration of the evolution from point 1 to point 2 for a $1M_\odot$ star is 7×10^9 years. (From Iben 1967a.)

A general tendency at all masses is that the luminosity increases during the central hydrogen burning. This may be understood in terms of the changes that take place in the core of the star. As hydrogen is converted into helium, the hydrogen abundance X decreases; hence, according to equation (3.27)^(11.4) the mean molecular weight μ increases.

^(11.4) or common sense: helium is heavier than hydrogen.

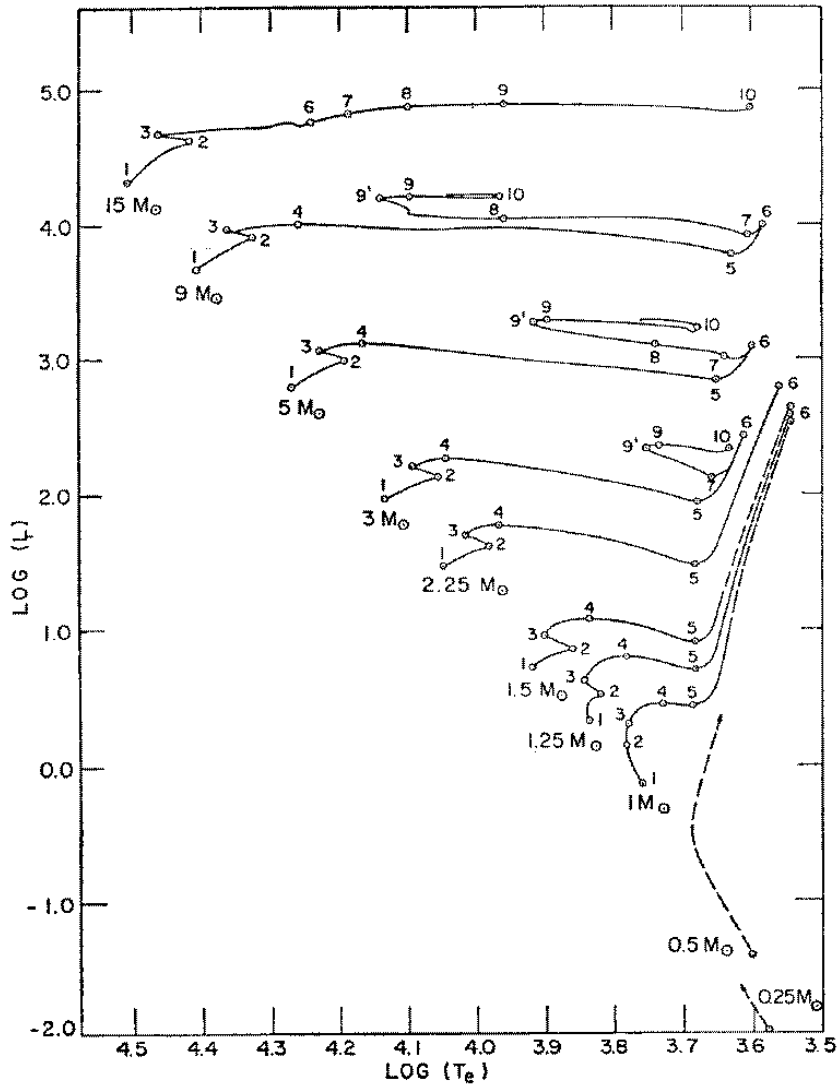


Figure 11.5. Evolutionary tracks in the Hertzsprung-Russell diagram for the evolution following the main sequence. The unit of luminosity L_s is $3.86 \times 10^{33} \text{ erg sec}^{-1}$, and the effective temperature T_e is in K. The models were computed with the composition $X = 0.708$, $Z = 0.02$. Tracks are shown for models of mass $M/M_\odot = 0.5, 1.0, 1.25, 1.5, 2.25, 3, 5, 9$ and 15 . Dashed portions of the evolutionary tracks are estimates. (From Iben 1967a.)

Since the pressure has to be sufficient to balance the weight of the overlying material and hence cannot decrease, it follows from the ideal gas law, equation (3.24), that ρT must increase to compensate for the increase in μ . In fact, the core contracts, thus increasing ρ . The contraction releases gravitational potential energy which, according to the virial theorem, goes partly towards increasing the internal energy of the gas; as a result the temperature increases. This tends to increase the nuclear energy generation rate, as does the increase in density; furthermore, the increase in temperature increases the radiative flux of energy, partly through the resulting reduction in opacity [*cf.* equations (5.6) and

(5.14)]. The result is that the luminosity of the star increases.

The steep increase in luminosity with increasing mean molecular weight was in fact already predicted in equations (7.7) and (7.8). There it followed exclusively from the changes in the radiative energy transport. In fact, there must be a balance between the energy production and the energy transport, which determines the equilibrium structure of the star; also, equations (7.7) and (7.8) essentially assumed a uniform chemical composition, whereas in fact the nuclear burning, and hence the change in μ , predominantly take place near the centre. Thus the dependence of luminosity on μ derived in section 7.1 cannot be used directly for an evolving star; however, the principles underlying the derivation in that section are rather similar to the discussion given above of the changes in the star as it evolves.

Exercise 11.1:

Review the derivation in section 7.1, and compare it with the discussion given here.

While the change in luminosity may be understood in fairly simple terms, as discussed above, the reasons for the variation in the other global properties of the star, *i.e.*, radius and effective temperature, are less obvious. In all cases the surface radius of the star expands as the star evolves, but at very different rates. For low masses the expansion is relatively modest; as a result the increase in luminosity leads to an increase in effective temperature [see equation (5.12)]. For higher mass, however, the expansion is more rapid, and the effective temperature decreases. The trend that core contraction is associated with surface expansion may be an example of a more general principle, as discussed in Chapter 12. There is no doubt about the correctness of the numerical results; however, the behaviour is so regular that one might expect an underlying mechanism that is sufficiently simple to be understandable, at least qualitatively.

Currently, no generally accepted explanation exists. However, to my mind, the most reasonable suggestion has been given by Douglas Gough, in an unpublished set of lecture notes. It was argued above that the virial theorem predicts the core contraction to lead to heating of the core. This, however, is strictly speaking an incorrect application of the virial theorem to just the core. In fact we need to consider the changes in the entire star, and the result provides a measure of the change of the total thermal energy, and hence some average of the temperature, rather than the change in the core temperature. It seems likely that if the entire star were to contract as a result of the core contraction, the decrease in the gravitational potential energy, and hence the increase in the thermal energy, would be so large that the core temperature would increase too much; the result would be an increase in the energy generation rate beyond what could be transported out through the star. Hence the outer parts of the star have to expand, to compensate for the contraction of the core, and hence keep the increase in core temperature at an acceptable level. Some support for this idea comes from the difference between low- and high-mass stars: for high-mass stars the energy generation is dominated by the highly temperature-sensitive CNO cycle; hence the acceptable increase in core temperature is smaller than at low stellar mass, and the required expansion is consequently larger.

This is clearly not a very compelling argument^(11.5), but it does provide a possible explanation for computed behaviour. Furthermore, the explanation might in principle be

^(11.5) I once attended a mathematics lecture in which an argument was described as being

tested by analyzing the computed models in detail. In fact, surprisingly little work has been done towards trying to understand the results of stellar evolution calculations in this manner. This would appear to be an interesting line of research.

11.3.2 The changes in the hydrogen abundance

The details of the way in which hydrogen is used up during core hydrogen burning have substantial effect on the subsequent evolution of the star. Because of the temperature sensitivity of the nuclear reactions, hydrogen is consumed most rapidly at the centre. In a star with radiative energy transport in the core, it is normally assumed that there is no core mixing^(11.6). It follows that helium produced by hydrogen burning remains where it is created, and hence the hydrogen abundance decreases most rapidly at the centre. The result is a variation of the hydrogen abundance with time and with location in the star such as is illustrated in Figure 11.6. In evolved stars X increases gradually from the centre, and complete exhaustion of hydrogen first occurs precisely at the centre.

Massive stars have convective cores, which are mixed on a timescale very short compared with the evolutionary timescale (*cf.* section 6.4.3). Hence within the convective cores the chemical composition can be assumed to be uniform at all times. As a result, the fusion of hydrogen to helium, which still predominantly takes place near the centre where the temperature is highest, leads to a uniform reduction in the hydrogen abundance in the convective core. The computations also show that the extent of the core generally shrinks as the star evolves; the most important reason for this is the reduction in the opacity, which may be assumed to be dominated by electron scattering, with the reduction in the hydrogen abundance [*cf.* equation (5.15)]. The result is the evolution in the hydrogen profile which is illustrated in Figure 11.7.

Figure 11.4 shows that for masses exceeding about $3M_{\odot}$ the convective core extends substantially beyond the region where the energy generation takes place. Hence, hydrogen is exhausted simultaneously throughout the nuclear-burning core. The consequences of this for the subsequent evolution of the star are discussed in Chapter 12.

11.3.3 The evolution timescale

The duration of the core hydrogen-burning phase is determined by the amount of hydrogen available for burning, and by the luminosity of the star. If q_c is the fraction of the stellar mass which takes part in the nuclear burning, and \bar{Q}_{eff} is the average amount of energy produced per generated helium atom, it follows from a relation similar to equation (8.49) that the duration of main-sequence phase may be estimated as

$$t_{\text{MS}} \simeq \frac{q_c X_0 \bar{Q}_{\text{eff}} M}{4\mathcal{A}_{\text{H}} m_{\text{u}} L_s}, \quad (11.1)$$

“not strong enough to hang a man”. The present argument is barely sufficient for handing out a parking ticket.

^(11.6) While not unreasonable, this assumption is not entirely obvious. It is possible that there are other sources of, possibly very slow, mixing, which could affect the composition of the cores of low-mass stars. On the other hand, there is no evidence for such mixing in the case of the Sun.

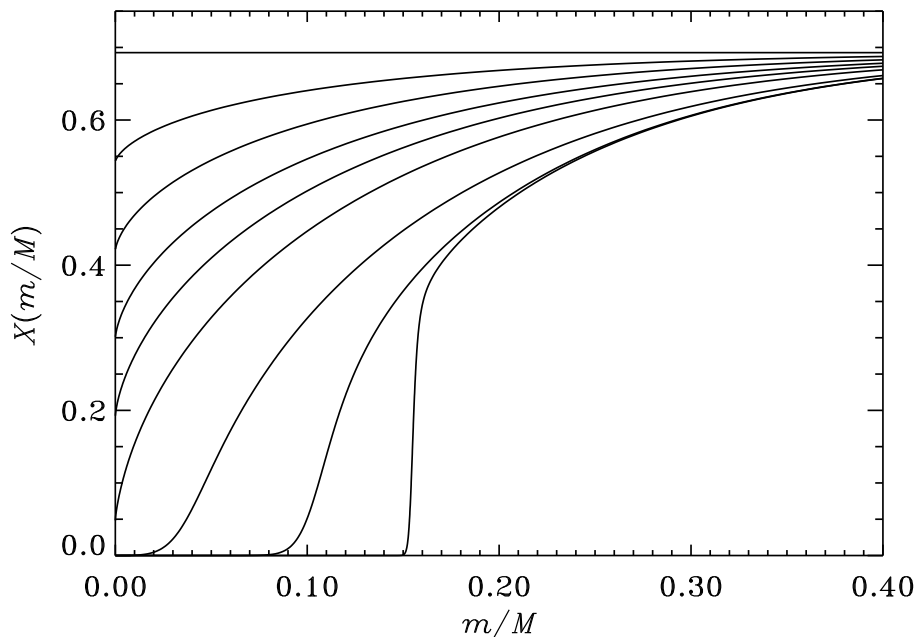


Figure 11.6. Hydrogen profiles showing the gradual exhaustion of hydrogen in a star of $1M_{\odot}$. The homogeneous initial model consists of a mixture with a hydrogen abundance by mass of 0.699. X as a function of the mass fraction m/M is plotted for nine models which correspond to ages of 0, 2.0, 3.6, 5.0, 6.2, 7.5, 9.6, 11.0 and 11.6 times 10^9 years, after the onset of hydrogen burning. The model at 5.0×10^9 years corresponds roughly to the present Sun, whereas the last two models are in the *shell hydrogen burning phase*, which is discussed in Chapter 12.

where X_0 is the initial hydrogen abundance. Assuming that q_c and \bar{Q}_{eff} are roughly independent of stellar mass, and that the mass-luminosity relation can be represented as $L_s \propto M^{\nu}$, we obtain^(11.7)

$$t_{\text{MS}} \propto M^{-(\nu-1)}. \quad (11.2)$$

From the estimates given in section 7.1 the exponent ν is 3 – 5 (see also Figure 11.4); hence the main-sequence lifetime decreases steeply with increasing mass. This is confirmed by the computed values given in Table 11.1.

^(11.7) In fact, the assumption of constant core mass fraction is rather dubious. In particular, it follows from Figure 11.4 that the extent of the convective core, and hence the fraction of the mass which may contribute fuel to the hydrogen burning, increases substantially with increasing stellar mass. A further uncertainty in estimates of the main-sequence lifetime is the extent of *overshoot* from the convective core: it is virtually certain that convective motion does not stop at the boundary of the convectively unstable region, but penetrates somewhat into the surrounding stable region; this increases the amount of hydrogen available for burning, but the extent of the penetration is very uncertain.

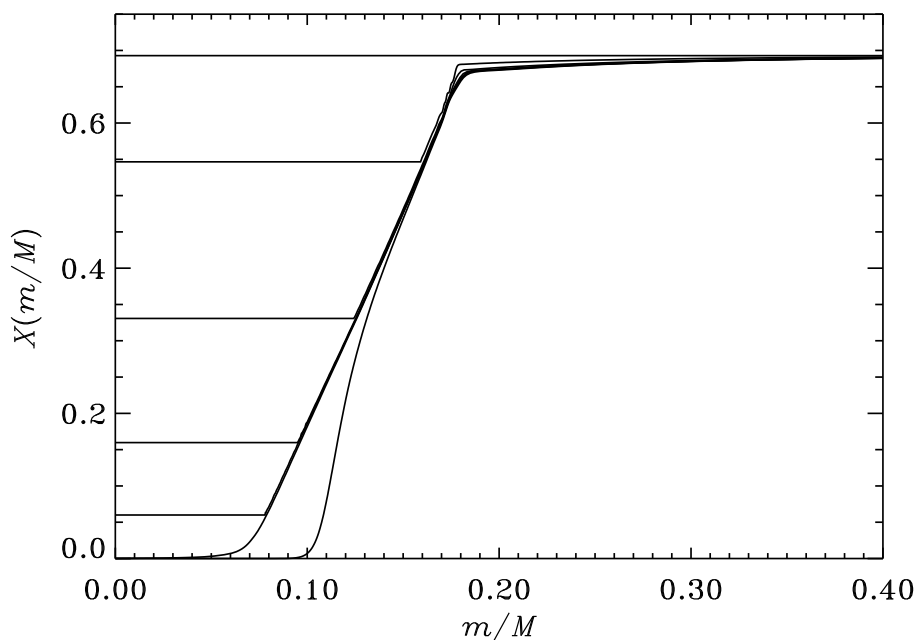


Figure 11.7. Hydrogen depletion in a $2.5M_{\odot}$ star with a shrinking convective core. The homogeneous initial model has $X = 0.699$. The lines show the hydrogen profiles for models of age 0, 1.5, 3.1, 4.0, 4.4, 4.6, and 4.8 times 10^8 years. Note that since hydrogen burning is negligible at the edge of the convective core during the main-sequence phase, the hydrogen profile established during this phase reflects the decrease in the extent of the core. In contrast, the last model is in the hydrogen shell-burning phase, the helium core having grown substantially beyond the smallest extent of the convective core.

11.4 The evolution of the Sun

11.4.1 Introduction

The computation of solar models follows the procedures discussed for other stars. However, a particular feature of the solar calculations is that the models should match the observed radius and luminosity of the present Sun, which are known with considerable precision. In fact, agreement with the observed values could have been regarded as a test of the computed models, were it not for the fact that the computations effectively contain two parameters, which are not known *ab initio* with sufficient precision: the abundance of helium in the initial Sun^(11.8), and a parameter determining the efficiency of convection

^(11.8) The helium abundance cannot be measured spectroscopically in the case of the Sun, because the solar photospheric spectrum does not contain helium lines. It is true that helium was first discovered in the Sun, but only in lines formed in the upper parts of the solar atmosphere; here conditions are so uncertain that the measured line strengths cannot be used for a reliable abundance determination. In contrast, fairly accurate observations have been made of the abundances of most other important elements in the Sun.

near the solar surface, where convection cannot be assumed to be essentially adiabatic. Given assumptions about the other physical parameters characterizing the solar model (in particular the opacity tables) these two parameters are adjusted until the model fits the observed radius and luminosity, at the age of the present Sun; the age has been estimated on the basis of radioactive age determinations for meteorites.

A typical example of a model of the present Sun is shown in Table 11.2. It differs from the models discussed so far by including also the effect of element diffusion and settling; in particular, there is a tendency for heavier elements including helium to sink towards the centre while hydrogen rises towards the surface. This effect is fairly weak in the Sun; even so, it causes a significant increase in the hydrogen abundance X in the convection zone, seen in Table 11.2, relative to the original abundance, $X_0 = 0.709$. As discussed in Section 11.5.2, this effect has been confirmed by observations of solar oscillations.

11.4.2 Changes during the evolution of the Sun

It is evident from Figure 11.5 that the $1M_\odot$ star shares the general trend of an increase in luminosity as the star evolves. To illustrate this in more detail, and to investigate the simplified analysis of the reasons for the increase which was given in section 11.3.1, Figure 11.8 shows the changes in a number of quantities during the evolution of a solar model from the ZAMS to the present age. The driver of the evolution is the decrease in the central hydrogen abundance X_c , from the initial value of 0.709 to the value of 0.335 in the present Sun. As argued in section 11.3.1 the resulting increase in the central mean molecular weight forces a core contraction, hence increasing the central density. This leads to an increase in the central temperature T_c . It is interesting, however, that the effect on the central energy generation rate ϵ_c is fairly modest; the increase in T_c should cause a substantially larger increase in ϵ_c due to the comparatively high temperature sensitivity of nuclear reactions; but this is largely compensated for by the decrease in the hydrogen abundance [since the energy generation is dominated by the PP chains, $\epsilon \propto X^2$; cf. equation (8.52)]. Also, there is a substantial reduction in the central opacity κ_c , caused by the increase in the temperature and the decrease in the hydrogen abundance. The combined effect of the increase in ϵ and the decrease in κ finally leads to the increase in the surface luminosity L_s ; the results show that L_s was approximately 30 per cent lower on the ZAMS than at present.

11.4.3 Climatic effects of solar evolution?

An obvious question is whether the climate of the Earth may have been affected by this increase in the luminosity of the Sun since it arrived on the main sequence. A simple estimate suggests that this may be possible. To maintain equilibrium, there must be a balance between the amount of heat received by the Earth from the Sun, and the amount of heat radiated by the Earth (if we neglect the heat generated by radioactive processes in the Earth's interior). If we assume that the Earth absorbs all the energy it receives, that the energy is redistributed evenly over the surface of the Earth (due to the rotation of the Earth, and the effects of winds and ocean currents), and that the Earth radiates as a black body with temperature T_E , the equilibrium terrestrial temperature may be estimated as

$$T_E = \left(\frac{L_\odot}{16\pi d^2 \sigma} \right)^{1/4} = \left(\frac{R_\odot}{2d} \right)^{1/2} T_{\text{eff},\odot}, \quad (11.3)$$

where d is the distance between the Sun and the Earth.

Table 11.2

$\frac{r}{R}$	$\frac{m}{M}$	$\frac{L_r}{L_s}$	X	$\log P$	$\log T$	$\log \rho$	κ	ϵ	$\frac{N_e}{N_{e,0}}$
0.000	0.000	0.000	0.335	17.371	7.195	2.188	1.24	16.99	1.000
0.020	0.001	0.007	0.350	17.359	7.191	2.174	1.26	16.54	1.000
0.040	0.007	0.053	0.385	17.326	7.180	2.135	1.30	15.07	1.000
0.060	0.020	0.153	0.434	17.274	7.163	2.080	1.36	12.96	1.000
0.080	0.044	0.293	0.488	17.208	7.142	2.013	1.44	10.58	1.000
0.100	0.076	0.452	0.540	17.131	7.117	1.941	1.54	8.20	1.000
0.120	0.118	0.602	0.585	17.045	7.090	1.866	1.65	6.04	1.000
0.140	0.166	0.729	0.622	16.952	7.061	1.789	1.77	4.23	1.000
0.160	0.220	0.826	0.650	16.852	7.032	1.710	1.90	2.82	1.000
0.180	0.277	0.894	0.670	16.747	7.002	1.628	2.05	1.82	1.000
0.200	0.336	0.938	0.684	16.637	6.972	1.543	2.21	1.13	1.000
0.250	0.482	0.988	0.702	16.346	6.900	1.319	2.69	0.33	1.000
0.300	0.610	0.999	0.708	16.041	6.832	1.081	3.31	0.05	1.000
0.350	0.712	1.000	0.712	15.734	6.769	0.837	4.10	0.01	1.000
0.400	0.790	1.000	0.713	15.433	6.709	0.595	5.10	0.00	0.999
0.450	0.848	1.000	0.715	15.141	6.653	0.359	6.29	0.00	0.996
0.500	0.890	1.000	0.716	14.861	6.600	0.131	7.71	0.00	0.993
0.550	0.921	1.000	0.717	14.591	6.548	-0.087	9.42	0.00	0.991
0.600	0.944	1.000	0.718	14.331	6.495	-0.295	11.54	0.00	0.991
0.650	0.960	1.000	0.719	14.076	6.439	-0.494	14.49	0.00	0.991
0.700	0.973	1.000	0.732	13.820	6.367	-0.681	19.26	0.00	0.991
0.750	0.983	1.000	0.737	13.547	6.260	-0.848	31.59	0.00	0.990
0.800	0.990	1.000	0.737	13.232	6.135	-1.038	50.94	0.00	0.989
0.820	0.992	1.000	0.737	13.089	6.079	-1.124	61.32	0.00	0.988
0.840	0.994	1.000	0.737	12.932	6.017	-1.218	74.83	0.00	0.988
0.860	0.996	1.000	0.737	12.757	5.947	-1.323	94.31	0.00	0.987
0.880	0.997	1.000	0.737	12.559	5.869	-1.442	1.2×10^2	0.00	0.986
0.900	0.998	1.000	0.737	12.328	5.777	-1.581	1.7×10^2	0.00	0.985
0.910	0.999	1.000	0.737	12.195	5.725	-1.660	2.1×10^2	0.00	0.984
0.920	0.999	1.000	0.737	12.048	5.667	-1.749	2.7×10^2	0.00	0.984
0.930	0.999	1.000	0.737	11.881	5.602	-1.849	3.8×10^2	0.00	0.982
0.940	1.000	1.000	0.737	11.688	5.526	-1.964	5.9×10^2	0.00	0.980
0.950	1.000	1.000	0.737	11.459	5.437	-2.102	1.1×10^3	0.00	0.977
0.960	1.000	1.000	0.737	11.176	5.328	-2.273	2.4×10^3	0.00	0.970
0.970	1.000	1.000	0.737	10.802	5.189	-2.500	8.0×10^3	0.00	0.954
0.980	1.000	1.000	0.737	10.256	4.998	-2.842	2.5×10^4	0.00	0.911
0.990	1.000	1.000	0.737	9.237	4.660	-3.489	1.3×10^5	0.00	0.800
0.992	1.000	1.000	0.737	8.875	4.565	-3.737	1.3×10^5	0.00	0.726
0.994	1.000	1.000	0.737	8.398	4.460	-4.084	7.4×10^4	0.00	0.617
0.996	1.000	1.000	0.737	7.741	4.343	-4.588	2.4×10^4	0.00	0.468
0.998	1.000	1.000	0.737	6.768	4.206	-5.368	4.1×10^3	0.00	0.280
0.999	1.000	1.000	0.737	6.063	4.115	-5.937	9.7×10^2	0.00	0.157
1.000	1.000	1.000	0.737	4.881	3.762	-6.699	0.34	0.00	0.000

Model of the present Sun (Model S of Christensen-Dalsgaard *et al.* 1996). The columns show: (1) distance from the centre in units of the surface radius; (2) mass in units of the total mass; (3) luminosity in units of the surface luminosity; (4) hydrogen abundance; (5) pressure P (dyn cm^{-2}); (6) temperature T (K); (7) density ρ (g cm^{-3}); (8) opacity κ ($\text{cm}^2 \text{g}^{-1}$); (9) the rate of energy generation ϵ ($\text{erg g}^{-1} \text{sec}^{-1}$); (10) the ratio between the number N_e of free electrons, and the total number of electrons $N_{e,0}$, per gram; this illustrates the transition from almost no ionization near the surface, where the ratio is zero, to complete ionization in the interior, where the ratio is 1.

The model was adjusted to have the observed surface radius of 6.96×10^{10} cm and the surface luminosity 3.846×10^{33} erg sec^{-1} at the age of the present Sun, which was taken to be 4.6×10^9 years. The model has an outer convection zone extending from just below the surface to $r/R = 0.711$.

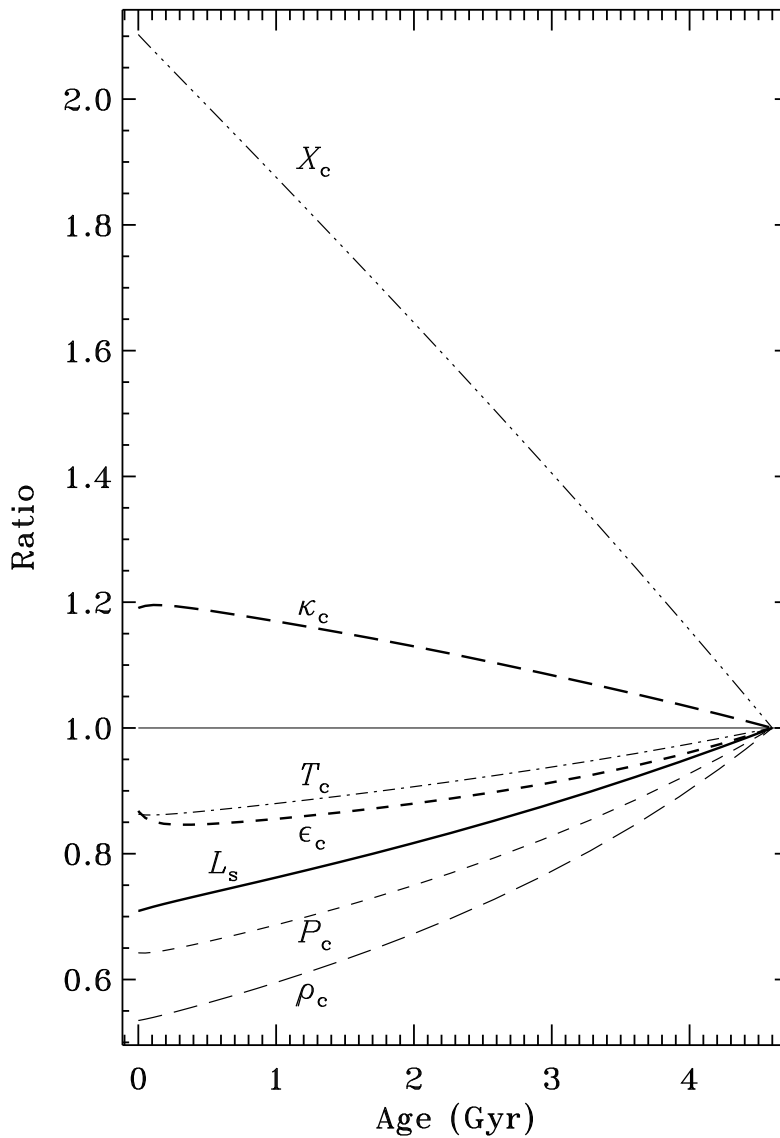


Figure 11.8. Variation in the surface luminosity and in properties at the centre during the evolution of a solar model. All variables have been normalized with their value in the present Sun. The heavy lines show the surface luminosity L_s (—————), the central energy generation rate ϵ_c (·····), and the central opacity κ_c (-----). The thin lines show the central density ρ_c (-----), the central pressure P_c (-----), the central temperature T_c (— · — · — ·), and the central hydrogen abundance X_c (·····).

Exercise 11.2:

Prove this relation. What is the predicted average temperature of the Earth?

According to equation (11.3), the initial average temperature of the Earth should have been about 7 per cent, or 20 K, lower than the present temperature, which is about 290 K. This suggests that the Earth may initially have been frozen over, in conflict with geological evidence which indicates development of life, almost certainly requiring liquid water, at least 3.5×10^9 years ago. Furthermore, with a substantial ice cover, the Earth would have reflected a large fraction of the incoming solar heat, further reducing the average temperature. Simple estimates of this effect suggest that if the Earth had at any time in its history been covered with ice, even an increase in the solar luminosity to a value substantially higher than the present would have been unable to melt the ice.^(11.9)

This so-called “faint early Sun” problem caused some discussion around the middle of the seventies, and attempts were made to produce solar models that did not display an increase in luminosity during main-sequence evolution. However, this increase is one of the most robust predictions of stellar evolution theory. As was discussed in sections 11.3.1 and 11.4.2, it results from the changes in structure caused by the depletion of hydrogen in the solar core. Even if the Sun were assumed to be completely mixed, thus increasing the supply of nuclear fuel and hence presumably decreasing the effects of evolution, a luminosity increase of about 20 per cent is still predicted. Under this assumption the dependence given in equation (7.7) of luminosity on mean molecular weight may be used to estimate the change in luminosity over the solar lifetime.

Exercise 11.3:

Assuming that the Sun has been fully mixed during its evolution, estimate the change in the hydrogen abundance from the ZAMS to the present. Then use equation (7.7) to estimate the change in the solar luminosity, assuming that the change in R can be ignored. The initial hydrogen abundance may be taken to be $X_0 = 0.7$, and the heavy element abundance is $Z = 0.02$.

Models with a constant solar luminosity can be constructed, but only by involving drastic modifications in the basic physics. One proposal which has been studied in some detail is to invoke a change with time in the gravitational constant G , and possibly the solar mass (for an example of this type of model, see Maeder 1977). Such changes have received no independent support, however, and are probably inconsistent with very accurate measurements of the motion in the solar system.

It should be noted, however, that the estimate given above of the change in the Earth’s temperature was extremely naive, in that it ignored all the complications of terrestrial climatology. In particular, it did not take into account the so-called *greenhouse effect*: the atmosphere of the Earth is largely transparent to radiation at wavelengths where most of the Sun’s energy is radiated; but because the temperature of the Earth is much lower, it radiates predominantly at much longer wavelengths [*cf.* equation (2.18)], and at these wavelengths there is strong absorption in the atmosphere, particularly due to certain molecules,

^(11.9) This argument is based on somewhat simplified models of the Earth’s climate. There have recently been suggestions that the Earth has in fact passed through episodes of nearly complete ice cover, which were reversed by a run-away greenhouse effect caused by volcanic release of CO_2 ; see, for example, Hoffman & Schrag (2000).

such as water vapour and carbon dioxide (CO₂). Hence the energy is partially trapped in the Earth's atmosphere, the degree of trapping depending on the abundance of CO₂^(11.10).

It is now clear that *if* there has been a suitable reduction in the abundance of CO₂ in the Earth's atmosphere during solar evolution, the decreasing efficiency of the greenhouse effect might have compensated for the increase in solar luminosity, keeping the temperature at the Earth's surface approximately constant. That this should be so could seem as an incredible coincidence. However, there are mechanisms which may link the absorption or release of CO₂ to the surface temperature of the Earth, in such a way that CO₂ is bound up, *e.g.* in rocks, if the temperature gets too high, thereby decreasing the efficiency of the greenhouse effect; and CO₂ is released if the temperature gets too low. There have even been speculations that these mechanisms could be of a biological nature, involving the photosynthesis in the plants and the metabolism in animals^(11.11). On the other hand, there appears to be also inorganic mechanisms which may provide the required feedback. A very interesting discussion of these questions was given by Kasting, Toon & Pollack (1988); they also analyzed the reasons for the striking differences between the climates of Venus, the Earth and Mars.

Computations of solar evolution show, as also indicated in Figure 11.5, that the solar luminosity will continue to increase. Hence, to maintain the same surface temperature the efficiency of the greenhouse effect should be reduced even further, by reducing the CO₂ abundance in the Earth's atmosphere. There is an obvious limit to how far this reduction may go. In fact Lovelock & Whitfield (1982) estimated that in approximately 150 million years the acceptable CO₂ abundance may become too low for photosynthesis to be possible. While this is no immediate cause for worry, the time estimate is nevertheless very short compared with the age of the Earth. There is a much more serious concern, however: currently the atmospheric CO₂ abundance is rising fairly rapidly, as a result of the burning of fossil fuel (coal and oil) and the reduction in the tree cover. As discussed by Schneider (1989) this may already have had effects on the Earth's climate, and it is virtually certain to lead to a significant increase in the temperature of the Earth over our lifetime, with very serious economical and sociological consequences. How to deal with this problem is one of the major challenges, to all of us, of the present time.

There is mounting evidence that the Sun affects the climate of the Earth (beyond the obvious effects) on shorter time scales also. This appears to be related to the magnetic activity of the Sun, leading to the appearance of sunspots the number of which varies roughly cyclically with a period around 11 years. During the period 1640 – 1710, however, where there were already fairly systematic observations of the Sun, the sunspots apparently almost disappeared; interestingly, this so-called *Maunder minimum* in solar activity coincides with the 'little ice age', an unusually cold period^(11.12). More quantitative evidence for a climatic effect has been obtained through careful analyses by Labitzke & van Loon (1993) and by Friis-Christensen & Lassen (1991); the latter authors found an apparently strong

^(11.10) A similar mechanism is responsible for the heating up of a greenhouse: glass is transparent to solar radiation, but absorbs and hence traps the radiation from the interior of the greenhouse.

^(11.11) This idea underlies the *Gaia hypothesis*, which has been proposed by J. E. Lovelock and L. Margulis; according to it, the entire biosphere should be regarded as a "living being", which adjusts condition so that they are optimal.

^(11.12) An unfortunate consequence of the cold winters was the ability of the Swedish army to cross the Danish belts over the ice during the war from 1657 – 1660, contributing significantly to the Danish defeat and hence to the loss of Scania (Skåne).

correlation between the *period* of the solar cycle and the temperature on the northern hemisphere, over the past few centuries. The physical mechanisms behind these correlations are not yet completely understood. An interesting possible cause was found by Svensmark & Friis-Christensen (1997) (see also Svensmark 1998), who showed that the cloud cover was strongly positively correlated with the intensity of the galactic cosmic rays; the propagation of cosmic rays through the solar system is affected by the solar wind and hence by solar activity, in such a way that the intensity of cosmic rays is decreased at periods of high solar activity.

These results have raised the question whether the consequences of the increasing greenhouse effect resulting from burning fossil fuel have already been seen in the Earth's climate, or whether any possible climatic changes in the past century can be blamed solely on the Sun (for a rather one-eyed, but enjoyable, presentation of the latter view, see Calder 1997). This debate is far from over. However, in any case it seems likely that both the Sun and human activities on Earth have the potential to affect the climate; thus restraint in the burning of fossil fuels and other production of greenhouse gasses seems well justified.

11.5 Tests of solar models

11.5.1 Introduction

In general it is difficult to obtain sufficiently detailed observations of an individual star to permit a careful test of computed models of the star. Hence much of the testing of stellar evolution calculations has been based on “statistical” properties of large groups of stars, particularly stars in open clusters. We return to this in Chapter 13. However, in the case of the Sun much more information is available. Here we present a brief discussion of two types of observations which, at least in principle, give information about the solar interior: the solar five-minute oscillations and the solar neutrinos. The results of using these data to test the computed models long appeared contradictory: the observed oscillation frequencies indicated that there are no major problems with our models of the Sun, while there were substantial differences between the computed and observed flux of neutrinos from the Sun. As is now known, this discrepancy was an indication that modifications were required in our description of the neutrino.

11.5.2 Solar oscillations

It is not possible here to present more than a very brief overview of the properties of solar oscillations, and what they have taught us about the solar interior. For more detailed descriptions the reviews by, for example, Leibacher *et al.* (1985), Libbrecht (1988), Gough & Toomre (1991), Harvey (1995) and Christensen-Dalsgaard (2002) may be consulted.

An oscillating string has many different *eigenmodes*, characterized by the number n of nodes, or places where the string does not move. Similarly there is a large number of different modes of oscillation of a star. However, while the oscillations of a one-dimensional object like a string can be characterized by a single number n , the characterization of the oscillations of a three-dimensional star requires three numbers. It may be shown that the variation of a mode of oscillation with co-latitude θ and longitude ϕ can be described in terms of a spherical harmonic $Y_l^m(\theta, \phi)$; hence two of the three wave-numbers characterizing the mode are the *degree* l and the *azimuthal order* m of the spherical harmonic. The third

wavenumber, the *radial order* n , describes the variation of the mode with the distance r to the centre of the star. To each mode of oscillation corresponds an *eigenfrequency* ν_{nlm} , such that for the mode the velocity, say, at a given point in the star varies with time as

$$\sin(2\pi\nu_{nlm}t). \quad (11.4)$$

In general the frequency depends on all three wave-numbers. However, it turns out that if rotation of the star is neglected, the frequencies are independent of m ^(11.13); we make this approximation and regard the frequencies ν_{nl} as being determined by just n and l .

It is straightforward to compute precise oscillation frequencies for a given stellar model. An example, for a model of the present Sun, is shown in Figure 11.9. The modes fall into three different categories:

- The *p modes* which are standing sound waves.
- The *f modes* which are essentially surface gravity waves.
- The *g modes* which are essentially internal gravity waves.

The frequencies depend on the structure of the model. For example, since the p modes are sound waves, their frequencies are largely determined by the speed of sound c in the stellar interior, which is given by

$$c^2 = \frac{\Gamma_1 P}{\rho} \simeq \frac{\gamma k_B T}{\mu m_u}; \quad (11.5)$$

the last approximation assumes the ideal gas law. Thus, frequencies of p modes may in principle give information about the temperature in stellar interiors; in practice, this requires some additional constraints on the chemical composition, and hence the mean molecular weight.

Of course, Figure 11.9 just shows the modes of oscillation that are *possible* in a given star (in the same way as for a string an infinite number of eigenmodes are possible). Whether any of these oscillations are actually seen in a given star depends on the mechanisms that excite and damp the oscillations. As discussed in section 2.8, in the case of the Sun a large number of modes are in fact excited, namely apparently modes in the frequency range between approximately 1500 and 5000 μHz , corresponding to periods between about 10 and 3 minutes, at all degrees from 0 to greater than 1000. The distribution of mode amplitude is largely independent of the degree l , and hence corresponds to the spectrum shown in Figure 2.9.

The observed frequencies ν_{nl} provide a very rich material against which to test the computed solar models. The analysis of these data, which in many ways are similar to seismic data for the Earth, is referred to as *helioseismology*. The results are somewhat surprising: for recent models the differences between computed and observed frequencies are generally less than 10 μHz . This is still considerable more than the estimated errors in the observations, which in some cases are less than 0.01 μHz ; but the agreement between computations and observations indicates that there are probably at least no gross errors in our computation of solar models. Hence we may also have some confidence in models of other main-sequence stars. Furthermore, the results of the comparison are quite sensitive to the details of the physics in the models. For example, the inclusion of Coulomb interaction in the equation of state led to a very significant improvement in the agreement between

^(11.13) Rotation introduces a splitting after m of the frequencies, rather similar to the Zeeman splitting of the energy levels of an atom in a magnetic field. This *rotational splitting* may be used to get information about the rotation in stellar interiors.

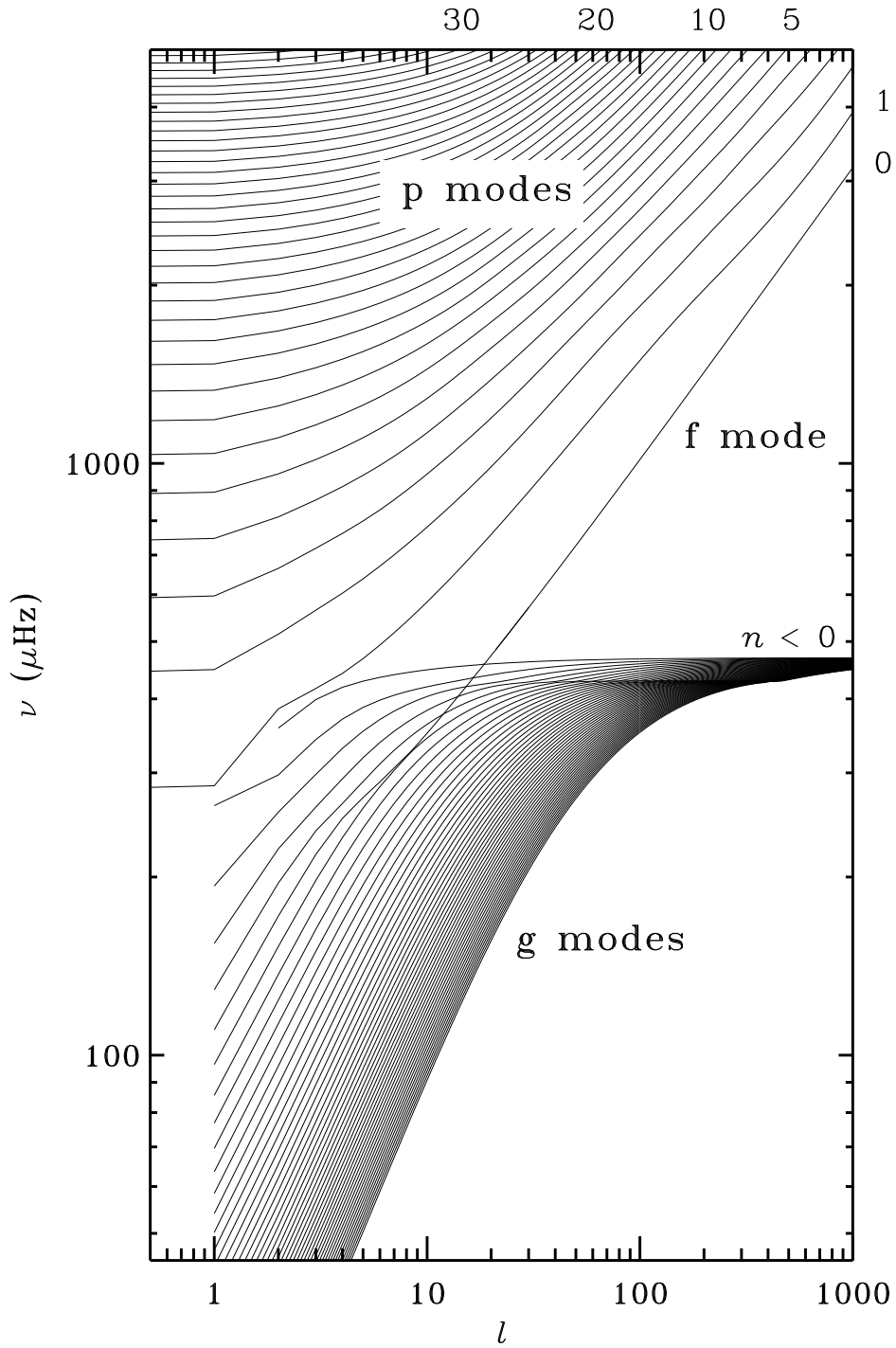


Figure 11.9. Computed frequencies of a solar model, as functions of the degree l . For clarity, points corresponding to a given value of the radial order n have been connected. Selected values of n are indicated.

computations and observations, Also, a ten per cent change in the assumed opacity in part of the Sun has a noticeable effect on the computed frequencies; analysis of the oscillation frequencies has indicated that the tabulated opacity near the base of the solar convection

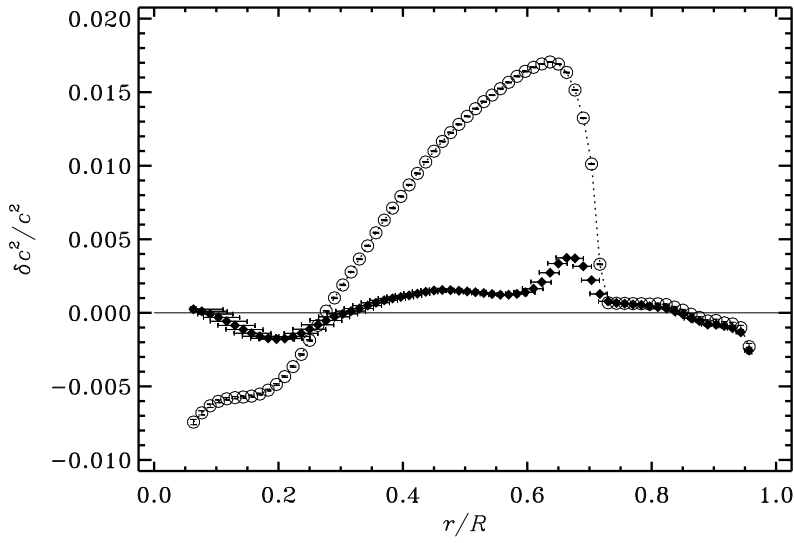


Figure 11.10. Relative difference in squared sound speed between the Sun and two solar models, obtained from analysis of observed frequencies of five-minute oscillations; the differences are shown in the sense (Sun) – (model). The open circles show results using a model without diffusion and settling, whereas the solid symbols were obtained with Model S (*cf.* Table 11.2) where diffusion and settling of helium and heavy elements were taken into account. The vertical error bars (barely visible) indicate the formal errors in the differences, based on the errors in the observed frequencies, whereas the horizontal bars provide a measure of the resolution in the determination.

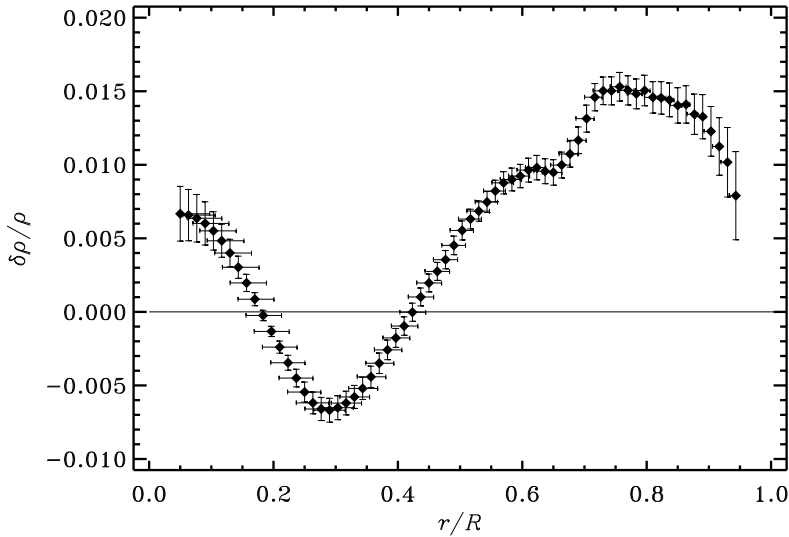


Figure 11.11. Relative difference in density between the Sun and Model S, obtained from analysis of observed frequencies of five-minute oscillations.

zone was too low, a result which has later been confirmed by new opacity computations. Thus observations of this nature may lead to improvements in the physics used in computing stellar models.

However, it is possible to go further than merely comparing observed and computed frequencies. By applying *inverse analysis* one may determine differences between the properties of the Sun and the model, from the differences between observed and computed frequencies. As examples Figures 11.10 and 11.11 show the relative differences in sound speed and density between the Sun and the model given in Table 11.2; in addition, sound-speed results for a model neglecting diffusion and settling are also shown. Without going into the detailed interpretation of the results, it is obvious that the sound speed in the model agrees quite precisely with the Sun; also, it is striking that the inclusion of settling, which in the past has often been neglected in solar modelling, leads to such a dramatic improvement in the agreement between the model and the Sun. The differences in density are somewhat larger than those in sound speed, especially in the convection zone. Nonetheless, given the simplifications made in computing the model it is perhaps surprising that it is so close to reality.

11.5.3 Solar neutrinos

As discussed in section 8.5, the production of one ${}^4\text{He}$ nucleus necessarily leads to the generation of two neutrinos. Since the neutrinos are virtually certain to escape for the Sun they may, at least in principle, be detected on the Earth. The measurement of the flux of neutrinos would then provide a direct measure of the rate of nuclear reactions in the core of the Sun.

To carry out this simple principle in practice involves numerous difficulties, however. The main problem is again the very small cross section of the neutrino, which makes it extremely hard to detect. Furthermore, the results that have been obtained over the past three decades have consistently been lower than the theoretically predicted values. This *solar neutrino problem* has led to a very large effort towards trying to modify the solar models with a view towards bringing the predicted neutrino flux into agreement with observations. A comprehensive discussion of the observations and model computations, and of the possible solutions to the problem, was given by Bahcall (1989). For more recent reviews, see, for example, Bahcall *et al.* (1995), Bahcall (1996), Castellani *et al.* (1997) and Kirsten (1999).

Here we give a summary of the principal features.

It follows from the analysis in section 8.5 that the neutrinos may be emitted in a number of different reactions, with very different energies. The distribution of the neutrinos depends on the branching ratios between the PP-I, PP-II and PP-III chains, and on the relative importance of the CNO cycle. Since the sensitivity of the neutrino detectors depends strongly on the neutrino energy, the observed number of neutrinos depends on the details of the neutrino spectrum. An example of a computed neutrino spectrum is shown in Figure 11.12.

The longest-running experiment to detect solar neutrinos, was established by R. Davis in the Homestake Gold Mine, South Dakota, in 1970 (for a recent overview of the results, see Cleveland *et al.* 1998); it uses the reaction



(*cf.* section 2.10). This reaction is in principle sensitive to neutrinos with energies exceeding about 0.8 MeV. In practice the predicted capture rate is dominated by the ${}^8\text{B}$ neutrinos,

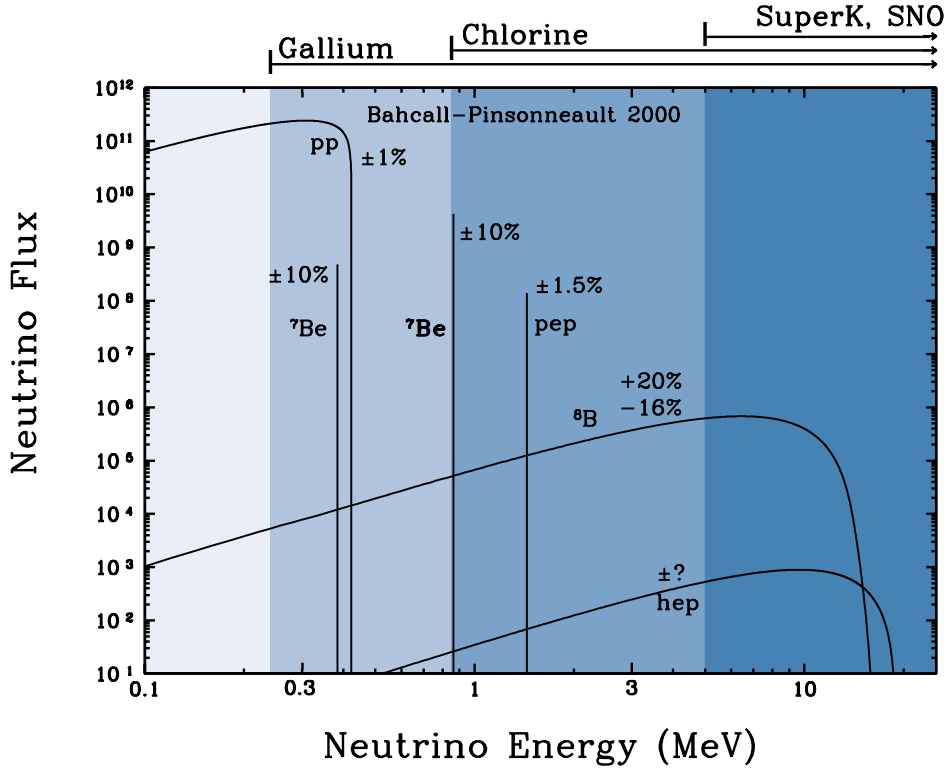


Figure 11.12. The energy spectrum of neutrinos predicted by a normal model of the present Sun. The neutrino fluxes from continuous sources are given in units of $\text{cm}^{-2} \text{sec}^{-1} \text{MeV}^{-1}$ at one astronomical unit; the line fluxes are in units of $\text{cm}^{-2} \text{sec}^{-1}$.

The spectra from the PP chains are shown with continuous lines: pp refers to the reaction ${}^1\text{H}({}^1\text{H}, e^+ \nu_e) {}^2\text{D}$, ${}^7\text{Be}$ to the reaction ${}^7\text{Be}(e^-, \nu_e) {}^7\text{Li}$, ${}^8\text{B}$ to the reaction ${}^8\text{B}(e^+ \nu_e) {}^8\text{Be}$, pep to the reaction ${}^1\text{H}({}^1\text{H} e^-, \nu_e) {}^2\text{D}$, and hep to the reaction ${}^3\text{He}({}^1\text{H}, \nu_e) {}^4\text{He}$ (note that the last two reactions were not discussed in section 8.5). In addition, modest contributions are made by the reactions in the CNO cycle. The shadings and the bars at the top of the figure indicate the ranges of sensitivity of the different techniques for detecting the neutrinos. (Adapted from Bahcall 1989.)

with the ${}^7\text{Be}$ neutrinos also making a significant contribution. On the other hand, the experiment is insensitive to the neutrinos emitted in the PP-I chain, which dominates the energy generation in the Sun. The predicted capture rates for this experiment from the different sources of neutrinos are listed in Table 11.3. The unit is *Solar Neutrino Unit*, or *SNU* which is defined as 10^{-36} captures per target atom in the detector per second. The total predicted capture rate is quoted by Bahcall (1989) as

$$\text{Predicted capture rate} = 7.9(1 \pm 0.33) \text{ SNU} , \quad (11.7)$$

where the indicated uncertainty takes into account the uncertainties in the model computations. More recent model calculations, including effects of settling and diffusion, give similar results: Bahcall & Pinsonneault (1995) found a rate of 9.3 SNU, whereas the prediction for Model S (*cf.* Table 11.2) is 8.2 SNU.

Table 11.3

Neutrino source	Capture rate (SNU)
pp	0.0
pep	0.2
hep	0.03
${}^7\text{Be}$	1.1
${}^8\text{B}$	6.1
${}^{13}\text{N}$	0.1
${}^{15}\text{O}$	0.3
${}^{17}\text{F}$	0.003
Total	7.9 SNU

The predicted capture rates for neutrinos from a normal solar model in the ${}^{37}\text{Cl}$ detector. (From Bahcall 1989.)

The measured capture rate is shown in Figure 11.13^(11.14). An average over these data gives

$$\text{Observed capture rate} = (2.05 \pm 0.3) \text{ SNU} ; \quad (11.8)$$

including more recent data the average is 2.56 SNU (Cleveland *et al.* 1998). Thus the predicted rates are clearly inconsistent with the measurements. This inconsistency constitutes the solar neutrino problem.

There have been suggestions that the measured rate might show a systematic, almost periodic, variation with time. This appeared to be anti-correlated with the solar cycle, such that the observed capture rate is large at solar minimum and small at solar maximum (*e.g.* Bahcall & Press 1991). It is likely that the correlation is spurious, however. It is very difficult to imagine how the variations during the solar cycle, which are normally assumed to take place in the solar convection zone, could influence the production rate of neutrinos. Also, statistical analysis of more extended data (Walther 1997) has failed to confirm the significance of the correlation. Finally, no significant variations of this nature have been found in other types of neutrino observations.

A second type of experiment to detect solar neutrinos uses scattering of the neutrinos on electrons in water. Since the electrons are predominantly scattered in the direction in which the neutrino arrives, this type experiment provides information about the direction to the source of neutrinos. Figure 11.14 shows the observed distribution as a function of the direction θ_{sun} to the Sun, compared with the predictions of a normal solar model; the measurements were made with the *Super-Kamiokande detector* in Japan, utilizing a tank of 50 000 tons of water buried deep in a mine. This provides the first evidence that neutrinos are actually coming from the Sun. The experiment is only sensitive to neutrinos of energy exceeding 6.5 MeV, *i.e.*, largely to the ${}^8\text{B}$ neutrinos. The results again show that the observed neutrino rate is smaller than the predicted rate (Fukuda *et al.* 1998a); a recent value for the ratio between measurements and predictions is 0.47.

^(11.14) It should be noted that the left-hand axis gives the argon production rate per day, as typically 0.5 atoms per day. In practice, the experiment is run for two months at a time, and the resulting roughly 30 argon atoms are collected and counted. Careful tests have shown that the methods used for extraction and counting are in fact able to detect such a small number of argon atoms accurately.

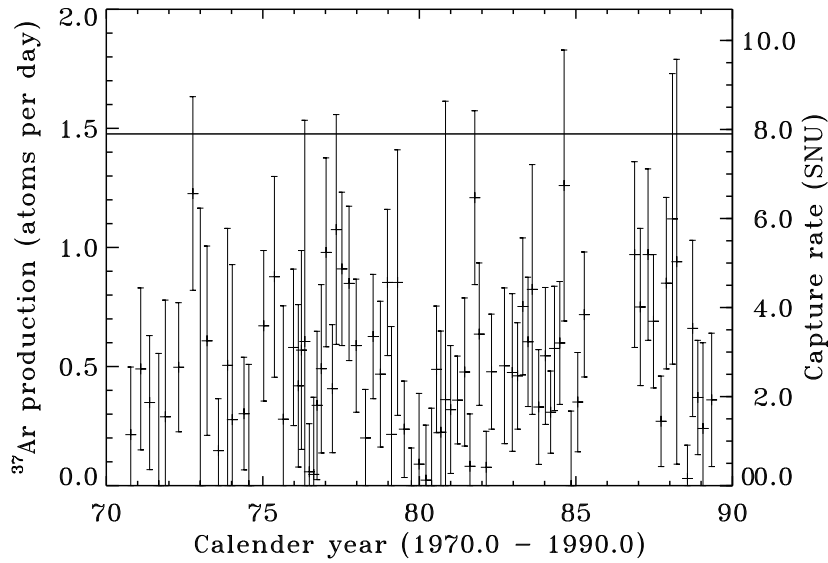


Figure 11.13. Observational results from the chlorine solar neutrino experiment. The line at 7.9 SNU across the top of the figure represents the prediction of a normal solar model. (Adapted from Bahcall 1989.)

These measurements of solar neutrinos led to the award of the 2002 Nobel prize in physics to Raymond Davis and Masatoshi Koshiba, for establishing, respectively, the ^{37}Cl and the Kamiokande experiments;^(11.15) they shared the prize with Riccardo Giacconi, who got his share for work in X-ray astronomy.

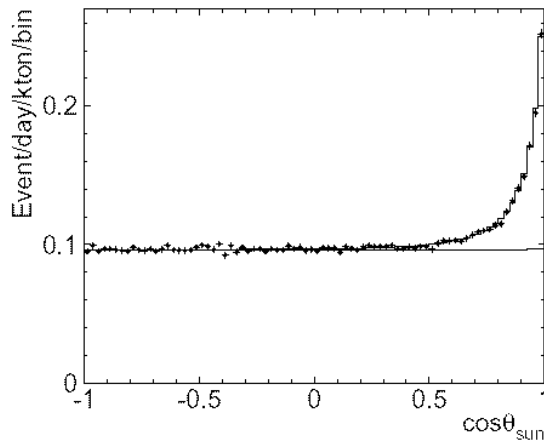


Figure 11.14. The distribution in $\cos\theta_{\text{sun}}$ (where θ_{sun} is the angle to the direction to the Sun) of neutrinos detected in an electron-scattering experiment. The histogram is the calculated distribution based on the predicted neutrino flux from a normal solar model. (See Fukuda *et al.* 2001.)

^(11.15) See Davis (2003; *Rev. Mod. Phys.*, **75**, 985) and Koshiba (2003; *Rev. Mod. Phys.*, **75**, 1011).

It should be noted that the neutrinos observed in these two experiments all come from the PP-II and PP-III chains. The electron-scattering experiment is only sensitive to the ^8B neutrinos from the PP-III chain, which also dominate the detections in the ^{37}Cl detector (*cf.* Table 11.3). Hence the predicted flux is very sensitive to the branching ratios between the PP-I, the PP-II and the PP-III chain, which in turn are highly sensitive to the central temperature of the Sun (see also exercise 8.8). Thus, to reduce the predicted capture rate to the observed value only requires a reduction in the core temperature of the Sun by about 5 per cent, while of course maintaining the correct total integrated energy generation rate and hence surface luminosity. It is possible to construct such models, although only by making fairly drastic modifications to the normal assumptions or parameters of stellar evolution calculations. However, in all cases considered so far the resulting models have oscillation frequencies which are inconsistent with the observed values (*cf.* section 11.4.3). As an example may be mentioned the suggestion that part of the energy transport in the solar core is carried out through the motion of hypothetical elementary particles, the so-called “Weakly Interacting Massive Particles” (or WIMPs). This would reduce the temperature gradient required to maintain radiative energy transport, and hence reduce the central temperature of the Sun. By a suitable choice of parameters it is possible to construct models which do indeed have the observed neutrino capture rate; furthermore, the effect on the structure of the model is fairly subtle, and hence, at the time where the suggestion was made, it was not obviously inconsistent with the observed oscillation frequencies. However, more careful observations (*e.g.* Elsworth *et al.* 1990) have convincingly demonstrated that while normal solar models are consistent with the observed frequencies, models with WIMPs are not. More generally, the excellent agreement between the sound speed in standard solar models and the Sun, found from helioseismology and extending well into the core where nuclear reactions take place (*cf.* Fig. 11.10) strongly suggests that the neutrino predictions of standard solar models are reasonably reliable (*e.g.* Bahcall *et al.* 1997).

It is obviously of great interest to carry out measurements that are sensitive to the basic pp neutrinos. Such measurements may be based on the reaction



which is sensitive to neutrinos of energy exceeding 0.23 MeV. Two such experiments have been carried out, using 30 and 60 tons of gallium (corresponding to a large fraction of the total World reserve). One of the experiments is the GALLEX experiment at the Gran Sasso in Italy (*e.g.* Anselmann *et al.* 1995); a recent compilation of the results of this experiment showed a capture rate of 78 ± 8 SNU (Kirsten 1999). The second experiment, the SAGE experiment at the Baksan Neutrino Observatory, found a capture rate of 67 ± 10 SNU (Abdurashitov *et al.* 1999), consistent with the GALLEX result. This is substantially below the total predicted value of around 135 SNU (*e.g.* Bahcall & Pinsonneault 1995), but consistent with the rate coming from the low-energy neutrinos produced in the PP-I chain.

Given the increasing precision of the solar oscillation measurements, it is difficult to imagine that a solar model can be found which is both consistent with the oscillation frequencies and with the neutrino capture rate. In view of the amount of oscillation data, and the ability to use these data to infer detailed properties of the Sun which are largely in agreement with the models, it appears most reasonable to assume that the structure of solar models is basically correct, and that the solution to the neutrino problem must be found elsewhere. A possible solution is the Mikheyev-Smirnov-Wolfenstein (or MSW) effect; it predicts that the electron neutrinos generated in hydrogen fusion may be transformed into neutrinos of different types, which are not detected in current experiments. The basis for

this effect is the existence of two additional types of neutrinos, in addition to the electron neutrino ν_e which has been considered so far: the *muon neutrino* ν_μ and the *tau neutrino* ν_τ . Neutrinos are normally considered to be mass-less; however, if the neutrinos have masses, and if the mass of the ν_e differs from that of the other types, it is possible that the ν_e neutrino may be transformed into a ν_μ or ν_τ through interaction with matter in the Sun. Of the experiments carried out so far, the electron-scattering experiment is predominantly sensitive to the ν_e , although with some sensitivity to the other types, whereas the ^{37}Cl and ^{71}Ga experiments are exclusively sensitive to ν_e . Thus, conversion of a substantial fraction of the ν_e to the other types may explain the observed deficit. The magnitude of the effect depends on the mass differences, and on parameters describing the interaction; however, it is possible to choose parameters such that the predictions are consistent with the observations (for an overview, see Bahcall, Krastev & Smirnov 1998). Some evidence for neutrino oscillations, involving the muon neutrinos, has been obtained from measurements of neutrinos produced in the Earth's atmosphere by reactions involving cosmic rays (*e.g.* Fukuda *et al.* 1998b; Kearns, Kajita & Totsuka 1999); this lends credence to the MSW effect as an explanation of the solar neutrino deficit.

Decisive tests of the mechanism have very recently come from the Sudbury Neutrino Observatory (SNO) which has started operations in Canada (see Boger *et al.* 2000). SNO measures solar high-energy (^8B) neutrinos through reactions with deuterium (^2H) in heavy water as well as through electron scattering. Of the two relevant reactions with ^2H , one (the so-called charged-current reaction) is sensitive exclusively to ν_e , whereas the second (the neutral-current reaction) has comparable sensitivity to all three types. The rate measured with the charged-current reaction may therefore be compared with the rate from previous electron-scattering measurements to deduce the number of ν_μ and ν_τ , to which the electron-scattering experiments also have some modest sensitivity. This provides a measure of the extent to which neutrino conversion has taken place and therefore allows an estimate of the original neutrino production rate in the solar core. The striking result is that the answer agrees, to within errors, with the predictions of standard solar models (Ahmad *et al.*, 2001). The decisive demonstration of neutrino conversion was obtained by Ahmad *et al.* (2002), who used SNO to measure the neutrino flux with the neutral-current reaction. The results yielded a flux at the Earth of ν_e of $(1.76 \pm 0.1) \times 10^6 \text{ cm}^{-2} \text{ sec}^{-1}$ and a flux of other neutrino types (ν_μ and ν_τ) of $(3.41 \pm 0.66) \times 10^6 \text{ cm}^{-2} \text{ sec}^{-1}$. This is again consistent with solar models, and furthermore provides strong constraints on the parameters controlling the neutrino conversions.

In parallel with these efforts to study neutrino conversion from solar observations, terrestrial experiments are carried. In a recent experiment, Eguchi *et al.* (2003) measured the flux of electron antineutrinos $\bar{\nu}_e$ from commercial nuclear reactors, and found strong evidence for neutrino oscillations. Other experiments are being developed that will direct beams of neutrinos from accelerators towards neutrino detectors, over distances of several hundred kilometers. However, the size of the Earth sets a natural limit to the scale of such experiments. Thus, observations of solar neutrinos remain a very important possibility for studying the properties of the neutrino experimentally, provided that conditions in the solar core can be determined with sufficient accuracy, from observations of solar oscillations, that the Sun can be regarded as a well-calibrated neutrino source.^(11.16)

^(11.16) Unfortunately, neutrino experiments suffered a serious setback in November 2001 when the Japanese Super-Kamiokande neutrino detector, measuring electron scattering in 50,000 tons of water, was seriously damaged. Repair is likely to take at least one, and possibly several, years. See *Nature*, **414**, 381 (2001).

References

- Abdurashitov, J. N., Bowles, T. J., Cherry, M. L., *et al.*, 1999. [Measurement of the solar neutrino capture rate by Sage and implications for neutrino oscillations in vacuum]. *Phys. Rev. Lett.*, **83**, 4686 – 4689.
- Ahmad, Q. R., Allen, R. C., Andersen, T. C., *et al.*, 2001. [Measurement of the rate of $\nu_e + d \rightarrow p + p + e^-$ interactions produced by ^8B solar neutrinos at the Sudbury Neutrino Observatory]. *Phys. Rev. Lett.*, **87**, 071301(1-6).
- Ahmad, Q. R., Allen, R. C., Andersen, T. C., *et al.*, 2002. [Direct evidence for neutrino flavor transformation from neutral-current interactions in the Sudbury Neutrino Observatory]. *Phys. Rev. Lett.*, **89**, 011301-(1 – 6).
- Anselmann, P., Hampel, W., Heusser, G., *et al.*, 1995. [GALLEX solar neutrino observations: complete results for GALLEX II]. *Phys. Lett. B*, **357**, 237 – 247.
- Bahcall, J. N., 1989. *Neutrino astrophysics*, Cambridge University Press, Cambridge.
- Bahcall, J. N., 1996. [Solar neutrinos: Where we are, where we are going]. *Astrophys. J.*, **467**, 475 – 484.
- Bahcall, J. N. & Pinsonneault, M. H., 1995. (With an appendix by G. J. Wasserburg). [Solar models with helium and heavy-element diffusion]. *Rev. Mod. Phys.*, **67**, 781 – 808.
- Bahcall, J. N. & Press, W. H., 1991. [Solar-cycle modulation of event rates in the Chlorine solar neutrino experiment]. *Astrophys. J.*, **370**, 730 – 742.
- Bahcall, J. N., Krastev, P. I. & Smirnov, A. Yu., 1998. [Where do we stand with neutrino oscillations?]. *Phys. Rev. D*, **59**, 096016-(1-22).
- Bahcall, J. N., Lande, K., Lanou Jr, R. E., Learned, J. G., Hamish Robertson, R. G. & Wolfenstein, L., 1995. [Progress and prospects in neutrino astrophysics]. *Nature*, **375**, 29 – 34.
- Bahcall, J. N., Pinsonneault, M. H., Basu, S. & Christensen-Dalsgaard, J., 1997. [Are standard solar models reliable?]. *Phys. Rev. Lett.*, **78**, 171 – 174.
- Boger, J., Hahn, R. L., Rowley, J. K., *et al.* (the SNO collaboration), 2000. [The Sudbury Neutrino Observatory]. *Nucl. Inst. Meth.*, **A449**, 172 – 207.
- Calder, N., 1997. *The manic Sun*, Pilkington Press.
- Castellani, V., Degl’Innocenti, S., Fiorentini, G., Lissia, M. & Ricci, B., 1997. [Solar neutrinos: Beyond standard solar models]. *Phys. Rep.*, **281**, 309 – 398.
- Christensen-Dalsgaard, J., 2002. [Helioseismology]. *Rev. Mod. Phys.*, **74**, 1073 – 1129.
- Christensen-Dalsgaard, J., Däppen, W., Ajukov, S. V., Anderson, E. R., Antia, H. M., Basu, S., Baturin, V. A., Berthomieu, G., Chaboyer, B., Chitre, S. M., Cox, A. N., Demarque, P., Donatowicz, J., Dziembowski, W. A., Gabriel, M., Gough, D. O., Guenther, D. B., Guzik, J. A., Harvey, J. W., Hill, F., Houdek, G., Iglesias, C. A., Kosovichev, A. G., Leibacher, J. W., Morel, P., Proffitt, C. R., Provost, J., Reiter, J., Rhodes Jr., E. J., Rogers, F. J., Roxburgh, I. W., Thompson, M. J., Ulrich, R. K., 1996. [The current state of solar modeling]. *Science*, **272**, 1286 – 1292.
- Cleveland, B. T., Daily, T., Davis Jr, R., Distel, J. R., Lande, K., Lee, C. K., Wildenhain, P. S. & Ullman, J., 1998. [Measurement of the solar electron neutrino flux with the Homestake chlorine detector]. *Astrophys. J.*, **496**, 505 – 526.
- Eguchi, K., Enomoto, S., Furuno, K., *et al.*, 2002. [First results from KamLAND: Evidence for reactor antineutrino disappearance]. *Phys. Rev. Lett.*, **90**, 021802-(1-6).
- Elsworth, Y., Howe, R., Isaak, G. R., McLeod, C. P. & New, R., 1990. [Evidence from solar seismology against non-standard solar-core models]. *Nature*, **347**, 536 – 539.

- Friis-Christensen, E. & Lassen, K., 1991. [Length of the solar cycle: an indicator of solar activity closely associated with climate]. *Science*, **254**, 698 – 700.
- Fukuda, S., Fukuda, Y., Ishitsuka, M., *et al.*, 2001. [Solar ^8B and hep neutrino measurements from 1258 days of Super-Kamiokande data]. *Phys. Rev. Lett.*, **86**, 5651 – 5655.
- Fukuda, Y., Hayakawa, T., Ichihara, E., *et al.*, 1998a. [Measurements of the solar neutrino flux from Super-Kamiokande's first 300 days]. *Phys. Rev. Lett.*, **81**, 1158 – 1162.
- Fukuda, Y., Hayakawa, T., Ichihara, E., *et al.*, 1998b. [Measurement of a small atmospheric ν_μ/ν_e ratio]. *Phys. Lett. B*, **433**, 9 – 18.
- Gough, D. O. & Toomre, J., 1991. [Seismic observations of the solar interior]. *Ann. Rev. Astron. Astrophys.*, **29**, 627 – 685.
- Harvey, J., 1995. [Helioseismology]. *Physics Today*, **48**, No. 10 (Oct.), 32 – 38.
- Hoffman, P. F. & Schrag, D. P., 2000. [Snowball Earth]. *Scientific American*, **282** (January), 50 – 57.
- Iben, I., 1967a. [Stellar evolution within and off the main sequence]. *Ann. Rev. Astron. Astrophys.*, **5**, 571 – 626.
- Kasting, J. F., Toon, O. B. & Pollack, J. B., 1988. [How climate evolved on the terrestrial planets]. *Scientific American*, **258** (February), p. 46 – 53 (US p. 90 – 97).
- Kearns, E., Kajita, T. & Totsuka, Y., 1999. [Detecting massive neutrinos]. *Scientific American*, **281** (August), 48 – 55.
- Kippenhahn, R. & Weigert, A., 1990. *Stellar structure and evolution*, Springer-Verlag, Berlin.
- Kirsten, A., 1999. [Solar neutrino experiments: results and implications]. *Rev. Mod. Phys.*, **71**, 1213 – 1232.
- Labitzke, K. & van Loon, H., 1993. [Some recent studies of probable connections between solar and atmospheric variability]. *Ann. Geophys.*, **11**, 1084 – 1094.
- Leibacher, J. W., Noyes, R. W., Toomre, J. & Ulrich, R. K., 1985. [Helioseismology]. *Scientific American*, **253**, (September) p. 34 – 43 (US p. 48 – 57).
- Libbrecht, K. G., 1988. [Solar and stellar seismology]. *Space Science Rev.*, **47**, 275 – 301.
- Lovelock, J. E. & Whitfield, M., 1982. [Life span of the biosphere]. *Nature*, **296**, 561 – 563.
- Maeder, A., 1977. [Four basic solar and stellar tests of cosmologies with variable past G and macroscopic masses]. *Astron. Astrophys.*, **56**, 359 – 367.
- Schneider, S. H., 1989. [The changing climate]. *Scientific American*, **261** (September), p. 38 – 46 (US p. 70 – 78).
- Svensmark, H., 1998. [Influence of cosmic rays on Earth's climate]. *Phys. Rev. Lett.*, **81**, 5027 – 5030.
- Svensmark, H. & Friis-Christensen, E., 1997. [Variation of cosmic ray flux and global cloud coverage—a missing link in solar-climate relationships]. *J. Atmos. Solar-Terr. Phys.*, **59**, 1225 – 1232.
- Walther, G., 1997. [Absence of correlation between the solar neutrino flux and the sunspot number]. *Phys. Rev. Lett.*, **79**, 4522 – 4524.